ARTICLES
https://doi.org/10.1038/s41567-021-01439-1
nature physics

Check for updates

OPEN

Enhancement of superexchange due to synergetic breathing and hopping in corner-sharing cuprates

Nikolay A. Bogdanov[1]✉, Giovanni Li Manni[1], Sandeep Sharma[1,2], Olle Gunnarsson[1] and Ali Alavi[1,3]✉

Cuprates with corner-sharing CuO_4 plaquettes have received much attention owing to the discoveries of high-temperature superconductivity and exotic states where spin and charge or spin and orbital degrees of freedom are separated. In these systems spins are strongly coupled antiferromagnetically via superexchange mechanisms, with high nearest-neighbour coupling varying among different compounds. The electronic properties of cuprates are also known to be highly sensitive to the presence, distance and displacement of apical oxygens perpendicular to the CuO_2 planes. Here we present ab initio quantum chemistry calculations of the nearest-neighbour superexchange antiferromagnetic (AF) coupling J of two cuprates, Sr_2CuO_3 and La_2CuO_4. The former lacks apical oxygens, whilst the latter contain two apical oxygens per CuO_2 unit completing a distorted octahedral environment around each Cu atom. Good agreement is obtained with experimental estimates for both systems. Analysis of the correlated wavefunctions together with extended superexchange models shows that there is an important synergetic effect of the Coulomb interaction and the O–Cu hopping, namely a correlated breathing-enhanced hopping mechanism. This is a new ingredient in superexchange models. Suppression of this mechanism leads to drastic reduction in the AF coupling, indicating that it is of primary importance in generating the strong interactions. We also find that J increases substantially as the distance between Cu and apical O is increased.

Although it has long been suspected that spin fluctuations play a crucial role in the extraordinary electronic properties of cuprates, important aspects of the antiferromagnetic interactions in these systems remain unclear. Key questions concern the reasons behind the very large AF couplings observed in cuprates, and how they can be accommodated within the accepted superexchange mechanism[1,2], as well as the role of apical oxygens. The strength of the AF coupling can be characterized by the nearest-neighbour (NN) coupling J, which enters in, for example, the Heisenberg model for undoped systems and the t–J model for doped systems[3]. Superexchange involves (virtual) electron hopping between Cu $3d$ and O $2p$ orbitals. Antiparallel spins on neighbouring Cu atoms allow for more hopping possibilities than parallel spins, leading to an AF coupling[2,4]. While the superexchange is well understood at the model level, the ab initio calculation of J is a major problem. For instance, calculations in a minimal though physically plausible active space underestimate J by almost an order of magnitude. This is therefore a long-standing problem in the ab initio community[5–10].

An exact wavefunction (WF)-based calculation[11] within the NN J model would involve correlating ~100 electrons among ~300 orbitals, leading to an eigenvalue problem in a Hilbert space of 10^{115} determinants. Since problems on such a scale are out of reach, we use the complete active space self-consistent field (CASSCF) method[12–14] together with multi-reference perturbation theories to systematically approximate the correlation energy. In the CASSCF(n,m) approach, a subset of n active electrons are correlated in a subset of m active orbitals, leading to a highly multi-configurational (CAS) reference WF. The choice of the active space will be discussed shortly, but let us note that, although the solution of the CAS WF is still an exponentially scaling problem, it is manageable with novel quantum chemistry methods, namely with full configuration interaction quantum Monte Carlo (FCIQMC)[15,16] and density-matrix renormalization group (DMRG)[14,17], as long as n and m are not too large. Additionally in the SCF process, all orbitals are self-consistently optimized in the field of the CAS WF, to yield the variational minimum. The CAS WF is then augmented using a number of second-order techniques, including n-electron perturbation theory (NEVPT2)[18,19], multi-reference linearized coupled cluster (MR-LCC2)[19,20] or multi-reference configuration interaction with single and double excitations (MR-CISD)[11]. These methods capture the remaining (weak) correlation involving electrons and orbitals outside of the active space. Using such approaches, it is possible, for example, to justify that the lowest electron removal state of La_2CuO_4 is the Zhang–Rice singlet state[21] and study it in detail[22]. We use a variety of second-order methods to gauge their reliability. As the active space is enlarged, the corresponding second-order corrections diminish. The key question that arises is: What is the 'minimal' active space necessary to obtain a qualitatively correct reference WF sufficient to compute J reliably? We find that the necessary active space needs to be far larger than previously imagined, including relatively high-energy Cu $4d$ and O $3p$ orbitals. Exclusion of these from the active space leads to a dramatic underestimation of J.

We analyse the reason for the strong dependence of J on the active space and, in particular, the importance of $4d$ orbitals. As mentioned above, the superexchange mechanism depends on O–Cu hopping. The Coulomb energy cost U_{eff} of this hopping is strongly reduced by an expansion of the Cu $3d$ orbitals, referred to as breathing[23], when an electron hops into a Cu $3d$ orbital. This breathing effect at the same time increases t_{eff}, the Cu–O effective hopping integral[24]. In a similar way, the O $2p$ orbital breathes as the O occupancy is changed. In the superexchange mechanism, J depends on both U_{eff} and t_{eff} (Supplementary Note 4) and the breathing effects therefore strongly influence J, as we shall shortly show.

The breathing effect involves a single $3d \rightarrow 4d$ excitation, leading to an *e*xpansion of the charge density when an electron is added to the d shell. There are also important double $3d3d \rightarrow 4d4d$ excitations,

[1]Max Planck Institute for Solid State Research, Stuttgart, Germany. [2]Department of Chemistry, University of Colorado Boulder, Boulder, CO, USA. [3]University Chemical Laboratory, Cambridge, UK. ✉e-mail: n.bogdanov@fkf.mpg.de; a.alavi@fkf.mpg.de

Table 1 | Values of the superexchange parameters *J* (meV) obtained with different methods

	Sr_2CuO_3		La_2CuO_4
	cc-pVDZ	cc-pVTZ	cc-pVDZ
CASSCF(2,2)	38	36	34
+MR-LCC2	97	96	78
+MR-CISD	69	65	55
+NEVPT2	107	106	85
+DDCI	246[a]	274	150[a]
CASSCF(4,3)[b]	38	37	35
+MR-LCC2	59	57	54
+MR-CISD	57	53	48
+NEVPT2	70	68	60
CASSCF(8,10)	70	69	50
+MR-LCC2	217	213	124
+MR-CISD	120	116	75
+NEVPT2	211	210	123
+CASPT2	260[a]	205	139[a]
CASSCF(24,26)	125	116	90
+MR-LCC2	252	256	147
+NEVPT2	253	262	149
CASSCF(28,30)[c]	143	139	93
+MR-LCC2	258	268	137
+NEVPT2	247	255	137
Experiment	249 (ref. [26]) 241 (ref. [27])		120 (ref. [28]) 138 (ref. [29])

[a]Ref. [7], calculations performed with different clusters and basis sets. [b]State-average CASSCF optimization is used here owing to otherwise present orbital ambiguity in triplet state. [c]Orbitals below O 2*p* were kept frozen after CASSCF(24,26).

which provide radial (in–out) correlations[11]. For a fixed number of *d* electrons, these correlations lead to a contraction of the charge density, at least if the basis has sufficient flexibility to satisfy the virial theorem. Correlation and breathing compete, making their simultaneous description complicated. Both effects lead to occupancy of 4*d* orbitals, but they are otherwise very different, and the ab initio calculations need to have the flexibility to capture both effects in a balanced way.

Ab initio calculations. To study the electronic structure of cuprates, we employ the embedded cluster model. With this approach, accurate high-level calculations are performed for a small representative unit of the solid, while its environment is treated in a more approximate manner[25]. The details of the employed model are presented in Methods section.

We first perform CASSCF calculations with two singly occupied Cu $3d_{x^2-y^2}$ orbitals in the active space CASSCF(2,2), similar to the one-band Hubbard model. Such minimal active-space calculations account for the unscreened Anderson superexchange mechanism (d^9–d^9 and d^8–d^{10} configurations) and give a qualitatively correct AF *J* coupling. The value of the *J* obtained this way is, however, only ~20% of experimental data[26–29] (Table 1). As can be seen, the second-order corrections nearly double *J*, but are clearly insufficient. The uniform behaviour of the different dynamical correlation methods suggests that the extended Hilbert space (CASSCF(2,2) reference WF plus second-order perturbation) is inadequate to qualitatively describe the system. Enlarging the reference WF represents a natural remedy to this problem. The only exception is the difference-dedicated configuration interaction (DDCI) method, which gives *J* values very close to experiment on top of CASSCF(2,2) reference[8,30]. However, the DDCI is essentially a subspace of the MR-CISD, and significant differences of *J* calculated by these two methods imply that the description of electronic structure given by DDCI is far from being complete.

Because an electron hopping from the bridging O σ-bonding $2p_y$ to the Cu $3d_{x^2-y^2}$ orbital plays a crucial role in the superexchange (see, for example, ref. [4]), this orbital is an obvious candidate to add into the active space. Such CASSCF(4,3) calculations roughly correspond to an unscreened multi-band Hubbard model. However, the obtained magnetic couplings turn out to be less than 1 meV higher compared with CASSCF(2,2). The reason is that, despite the inclusion of important ligand-hole determinants (d^9–p^5–d^{10} and d^{10}–p^4–d^{10}), their energies are too high to be effective because the orbital optimization is primarily driven by the dominant d^9–p^6–d^9 configuration[5,7,30]. When we include the effect of further excited determinants at second-order level on top of the CASSCF(4,3) WF, *J* is still much smaller than the experimental value, indicating that important correlation effects are still missing.

To effectively lower the energy of d^9–p^5–d^{10}, d^8–p^6–d^{10} and d^{10}–p^4–d^{10} determinants, one has to take into account orbital relaxation that comes along with them[5,7]. This can be done by adding a proper set of orbitals previously kept empty to the active space, namely Cu 4*d* and O 3*p*. Having additional *d* orbitals in the active space has been shown to be necessary to describe multiplet splittings for the late transition metals of the first row (see, for example, refs. [31–33]).

Because of the variationality of the orbital optimization within the CASSCF procedure, the active orbitals are allowed to change, and a balanced choice of active space is required to ensure convergence. Such a balanced active space can be constructed with Cu 3*d* and 4*d* orbitals with e_g character plus the bridging oxygen $2p_y$ and $3p_y$ orbitals[7] (Fig. 1, top three rows). Results for such CASSCF(8,10) calculations are shown in the third block of Table 1. The extension of the active space leads to a systematic differential effect with *J* increasing significantly at all levels of theory. Results close to experiment were reported using this active space together with a different formulation of the perturbation theory[7], but our calculation results are about 80% of experimental values. To achieve a balanced description of all relevant effects, we consider all copper 3*d* and 4*d* orbitals, together with the bridging oxygen 2*p* and 3*p* orbitals, resulting in CASSCF(24,26). This active space yields a diagonalization problem in a space of ~10^{14} Slater determinants, which we treat with DMRG and FCIQMC as approximate solvers[13,14]. With the additional many-body contribution from the Cu t_{2g} and π-bonding O orbitals taken into account in the large CASSCF, we find further stabilization of the singlet compared with the triplet. Second-order correction on top of the CASSCF(24,26) reference finally brings *J* close to the experimental values (see corresponding block in Table 1). The active orbitals are shown in Fig. 1; note that both 3*d* and 4*d* orbitals have significant amplitudes at the bridging oxygen *p* orbitals.

To verify that *J* values are converged with respect to the active space size, we performed even larger computations. We further correlated the peripheral O x^2-y^2-like 2*p* and 3*p* orbitals, the latter being strongly mixed with Cu 4*s* (Fig. 1). The last block in Table 1 shows the results of these CASSCF(28,30) calculations. The obtained *J* values are indeed close to the CASSCF(24,26) ones, with a slightly larger fraction being captured by CASSCF itself and less by the perturbation theory correction.

In a simple theory of superexchange[1,2], a model of Cu_2O is treated with one non-degenerate orbital on each atom. As discussed above, including only these orbitals in CASSCF(4,3) underestimates *J* by almost one order of magnitude. We now discuss why it is necessary to consider the large active space.

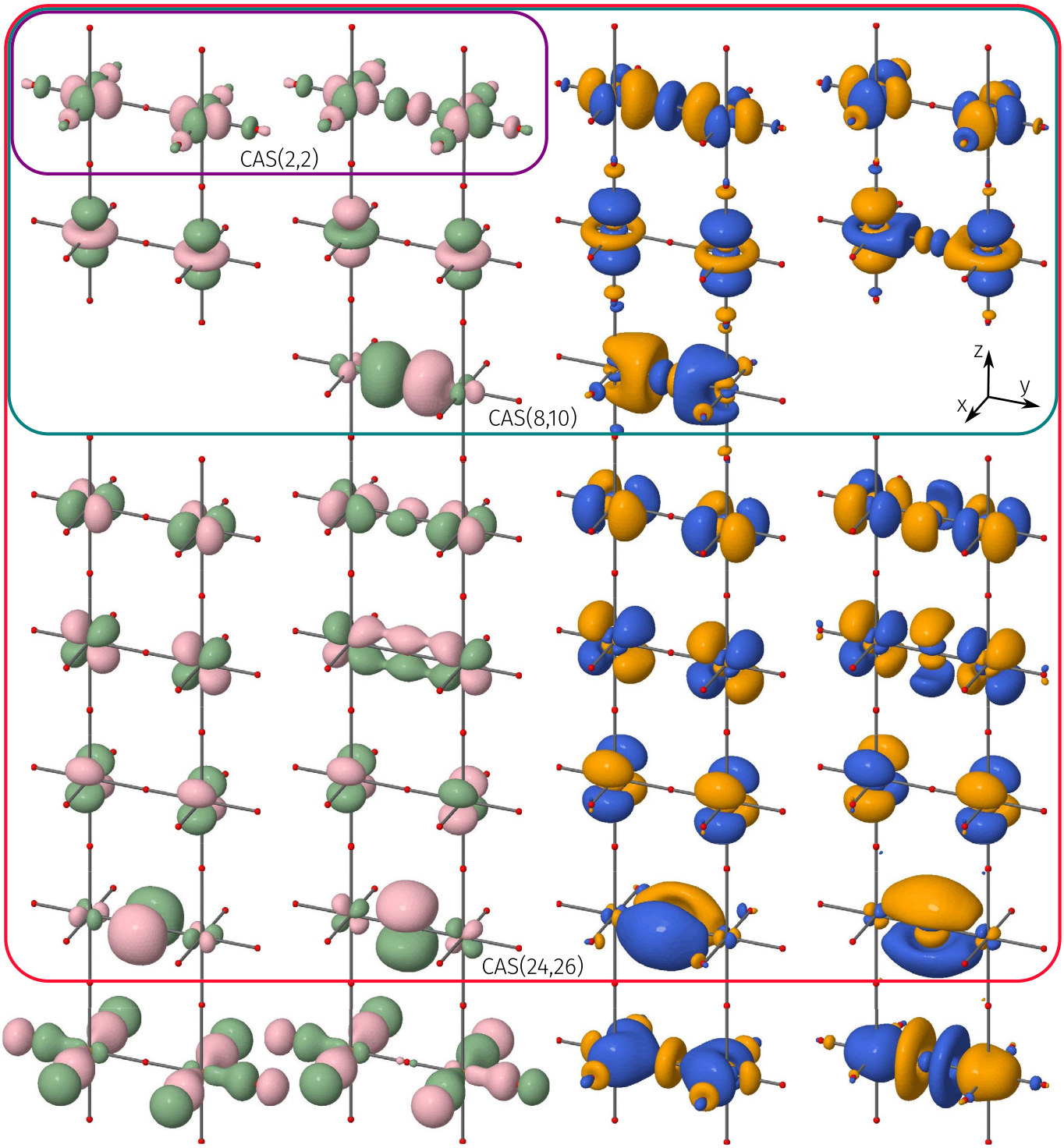

Fig. 1 | Orbitals explicitly correlated and optimized in CASSCF(28,30) calculations for the singlet state of La_2CuO_4 compound. Orbitals active in CASSCF(2,2), CASSCF(8,10) and CASSCF(24,26) calculations are indicated by smaller rectangles. Pink and green (yellow and blue) colours indicate phases of orbitals that are occupied (empty) at CASSCF(2,2) level.

Effective model. It is instructive to discuss the breathing effect in a very simple model, with an effective hopping directly between two Cu atoms that simulates the actual superexchange via bridging O. We show how the radial extent of the Cu 3*d* orbital is effectively increased in intermediate states with increased 3*d* occupancy. This has two important consequences. First, the effective energy cost of increasing the occupancy of 3*d* level is reduced, since the electrons can avoid each other better[23]. Second, the hopping between the two sites is enhanced, as the Cu 3*d* orbital expands[24].

As in the CASSCF calculations, we use a fixed orthogonal basis set for all intermediate states. Therefore the breathing effect of a 3*d* orbital is described as a mixing of the 3*d* and 4*d* orbitals. The system can effectively expand or contract an effective 3*d* orbital, being a linear combination of a 3*d* and a 4*d* orbital, depending on their relative sign.

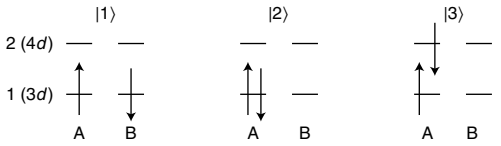

Fig. 2 | Schematic representation of states in equation (3).

To illustrate how this happens, we consider a Cu_2 dimer, including just one $3d$ and one $4d$ level on each atom, as indicated in Fig. 2. The levels have spin but no orbital degeneracy. We use the Hamiltonian

$$H = \sum_{\sigma}\left[\sum_{L}^{A,B}\sum_{i=1}^{2}\varepsilon_i n_{Li\sigma} + \sum_{i=1}^{2}\sum_{j=1}^{2} t_{ij}\left(c^{\dagger}_{Ai\sigma}c_{Bj\sigma} + c^{\dagger}_{Bi\sigma}c_{Aj\sigma}\right)\right] + \sum_{L}^{A,B}\left[U_{11}n_{L1\uparrow}n_{L1\downarrow} + U_{22}n_{L2\uparrow}n_{L2\downarrow} + U_{12}\sum_{\sigma\sigma'}n_{L1\sigma}n_{L2\sigma'}\right] + \sum_{L}^{A,B}\sum_{\sigma}\left(K_1 n_{L1\sigma} + K_2 n_{L2\sigma}\right)\left(c^{\dagger}_{L1\bar{\sigma}}c_{L2\bar{\sigma}} + c^{\dagger}_{L2\bar{\sigma}}c_{L1\bar{\sigma}}\right). \quad (1)$$

The first index on $c_{Li\sigma}$ refers to the site, and the second labels the orbital. That is, $i=1(2)$ refers to a $3d$ ($4d$) orbital. The hopping between the Cu atoms is described by t_{ij}. We include the direct on-site Coulomb integrals U_{11}, U_{12} and U_{22}, describing $3d$–$3d$, $3d$–$4d$ and $4d$–$4d$ interaction, respectively. K_i refers to a Coulomb integral with three equal orbitals and the fourth different:

$$K_i = e^2\int \mathrm{d}^3r\int \mathrm{d}^3r'\,\frac{\phi_i(\mathbf{r})^2\phi_1(\mathbf{r}')\phi_2(\mathbf{r}')}{|\mathbf{r}-\mathbf{r}'|}. \quad (2)$$

These integrals are crucial for the breathing effect. If, for example, the $3d$ orbital on an atom is doubly occupied, the last term in equation (1) can excite a single electron from the $3d$ orbital ϕ_1 to the $4d$ orbital ϕ_2. The effect of breathing is already evident in the atom (Supplementary Note 3). For simplicity, we here put $t_{12}=t_{21}=-\sqrt{t_{11}t_{22}}$, $U_{12}=\sqrt{U_{11}U_{22}}$ and $K_1/K_2=\sqrt{U_{11}/U_{22}}$. We have used $\varepsilon_2-\varepsilon_1=24$ eV, $U_{11}=13$ eV, $U_{22}=10$ eV, $K_1=-8$ eV, $t_{11}=-0.5$ eV and $t_{22}=-0.8$ eV.

Table 2 presents the singlet–triplet splitting obtained by solving the Hamiltonian in equation (1). It illustrates how inclusion of the integral K_1 strongly increases the splitting, because of breathing effects. To understand these results better, we consider a simpler calculation within only three configurations for the singlet state:

$$\begin{aligned}|1\rangle &= \tfrac{1}{\sqrt{2}}\left(c^{\dagger}_{A1\uparrow}c^{\dagger}_{B1\downarrow} + c^{\dagger}_{B1\uparrow}c^{\dagger}_{A1\downarrow}\right)|\mathrm{vac}\rangle\\ |2\rangle &= \tfrac{1}{\sqrt{2}}\left(c^{\dagger}_{A1\uparrow}c^{\dagger}_{A1\downarrow} + c^{\dagger}_{B1\uparrow}c^{\dagger}_{B1\downarrow}\right)|\mathrm{vac}\rangle\\ |3\rangle &= \tfrac{1}{2}\left(c^{\dagger}_{A1\uparrow}c^{\dagger}_{A2\downarrow} + c^{\dagger}_{A2\uparrow}c^{\dagger}_{A1\downarrow} + c^{\dagger}_{B1\uparrow}c^{\dagger}_{B2\downarrow} + c^{\dagger}_{B2\uparrow}c^{\dagger}_{B1\downarrow}\right)|\mathrm{vac}\rangle,\end{aligned} \quad (3)$$

where $|\mathrm{vac}\rangle$ is the vacuum state with no electrons. These configurations are shown schematically in Fig. 2. $|1\rangle$ corresponds to the d^9–p^6–d^9 configuration mentioned above, while $|2\rangle$ and $|3\rangle$ resemble the d^8–p^6–d^{10} configuration without and with $4d$ occupation, respectively. The Hamiltonian in equation (1) within the basis given by equation (3) reads

$$H = \begin{pmatrix} 2\varepsilon_1 & 2t_{11} & \sqrt{2}t_{12}\\ 2t_{11} & 2\varepsilon_1+U_{11} & \sqrt{2}K_1\\ \sqrt{2}t_{12} & \sqrt{2}K_1 & \varepsilon_1+\varepsilon_2+U_{12}\end{pmatrix}. \quad (4)$$

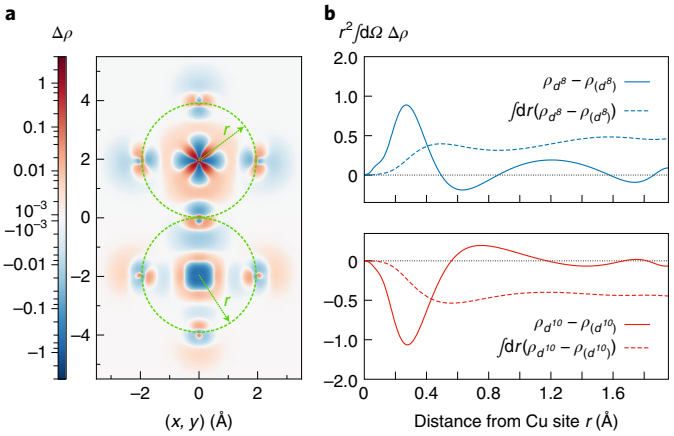

Fig. 3 | Electron density difference (in atomic units) due to orbital relaxation in the d^8–p^6–d^{10} configuration. a, Electron density difference in the plane of CuO_4 plaquettes. **b**, Electron density difference integrated over a sphere centred on one of the Cu atoms (full curves) as a function of the radius shown in **a**; the result of an additional radial integration (dashed curves) as a function of the upper integration limit.

Table 2 | Triplet–singlet splitting without ($K_1=0$) and with breathing (all values in eV)

K_1	Exact, equation (1)	Equation (4)
0	0.077	0.076
−8	0.182	0.172

Diagonalizing this matrix, we obtain the second column of Table 2. These results agree rather well with the full calculation for the model in equation (1), although the basis set in equation (3) is incomplete. The splitting is smaller because the higher-energy configurations have been neglected.

We can now use Löwdin folding, focusing on the upper 2×2 corner of $(H-z)^{-1}$

$$(H-z)^{-1} = \begin{pmatrix} 2\varepsilon_1 - 2t_{12}^2/\Delta E - z & 2t_{11} - 2t_{12}K_1/\Delta E\\ 2t_{11} - 2t_{12}K_1/\Delta E & U_{11} - 2K_1^2/\Delta E\end{pmatrix}^{-1}, \quad (5)$$

where $\Delta E=\varepsilon_2-\varepsilon_1+U_{12}$ and we have introduced the approximation $z\approx2\varepsilon_1$ in some places. The matrix in equation (5) shows rather clearly that there is an interference between breathing and hopping from the $3d$ orbital on one site and the $4d$ orbital on the other site.

The effective value of U has now been reduced,

$$U_{11}\rightarrow U_{11}^{\mathrm{eff}} \equiv U_{11} - 2\frac{K_1^2}{\Delta E}, \quad (6)$$

while the effective hopping has been increased,

$$t_{11}\rightarrow t_{11}^{\mathrm{eff}} \equiv t_{11} - \frac{t_{12}K_1}{\Delta E}, \quad (7)$$

since $K_1<0$ and t_{11} and t_{12} have the same sign. For the triplet case, the basis state $|2\rangle$ does not exist, and these renormalization effects are not present. The singlet–triplet splitting is then

$$E_{\mathrm{T}} - E_{\mathrm{S}} \approx \frac{4(t_{11}-t_{12}K_1/\Delta E)^2}{U_{11}-2K_1^2/\Delta E} \equiv 4\frac{\left(t_{11}^{\mathrm{eff}}\right)^2}{U_{11}^{\mathrm{eff}}}. \quad (8)$$

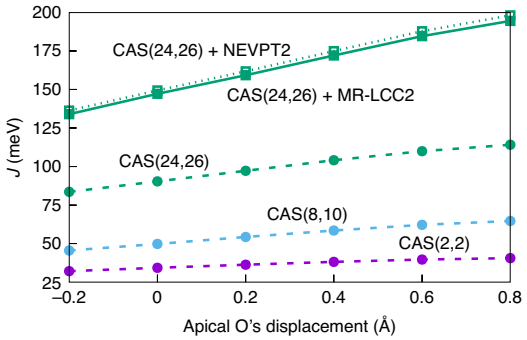

Fig. 4 | Dependence of J on the distance to apical oxygens in La_2CuO_4.

This illustrates the importance of the renormalization of both U_{11} and t_{11} by the breathing effect.

The presented model only includes non-degenerate d orbitals. Including the full five-fold degeneracy increases the renormalization of U by approximately a factor of five. The model has only $3d$–$3d$ hopping, but it illustrates the breathing effects. The more realistic case of $3d$–$2p$–$3d$ hopping results in a more complex expression for J where renormalization of t and U cannot be disentangled (Supplementary Note 4).

Reduction of *U*. The calculated bare on-site Coulomb integral between two $3d$ electrons is very large (~28 eV), leading to drastically suppressed charge fluctuations in the simplest model. For this reason, the CASSCF(2,2) and CASSCF(4,3) calculations give a very small J. However, by increasing the active space size, this energy cost can be strongly reduced. Crucial effects are the change of the effective radial extent of the $3d$ orbital (breathing) and rearrangements of the non-$3d$ charge density as the number of $3d$ electrons varies (screening)[23], which are captured in the CASSCF(24,26) calculation with second-order correction.

To disentangle these different effects, we performed a series of simpler, constrained calculations[34]. We put all hopping integrals from d ($3d$ or $4d$) basis functions on the Cu atoms equal to zero. We can then prescribe the total occupancy of d orbitals on each Cu atoms. We performed two calculations, one with the configuration d^9–p^6–d^9 and one with d^8–p^6–d^{10}. In both cases, the system is allowed to relax fully, except that hopping to or from d orbitals is suppressed. We then obtain that the energy of the d^8–p^6–d^{10} state is higher than the d^9–p^6–d^9 by 10–13 eV depending on initial conditions of constrained calculations (Supplementary Note 2). This means that bare $U \approx 28$ eV has been reduced to $U_{\mathrm{eff}} \approx 10$ eV. Experimental[35] and theoretical estimates[36–39] suggest that U_{eff} is reduced even further (~8 eV). This may be owing to more long-ranged effects left out in our finite-size cluster calculation.

Figure 3 shows charge differences due to breathing and screening for the d^8–p^6–d^{10} calculation, discussed above. A calculation was first performed for the d^9–p^6–d^9 state, then a d electron was moved from one Cu atom to the other, keeping all orbitals unchanged. The corresponding densities at two copper sites are denoted $\rho_{(d^8)}$ and $\rho_{(d^{10})}$. This d^8–p^6–d^{10} state is then allowed to relax self-consistently, giving the densities ρ_{d^8} and $\rho_{d^{10}}$. The solid red curve in Fig. 3b shows the change in the charge density $\rho_{d^{10}} - \rho_{(d^{10})}$, illustrating how charge is moved from the inner part of Cu to the outer part (breathing). The dashed red curve shows the radial integral of the charge density difference, revealing that more charge is removed from the inner part than is added to the outer part. Since the number of d electrons is the same in the two calculations, non-d charge has been moved away from the Cu atom with the d^{10} configurations as a response to the addition of one d electron (screening). Adding a d electron to a Cu atom thus only leads to an increase of the net charge by about half an electron, because of screening, which substantially reduces the energy cost.

Dependence of *J* on position of apical oxygens. As seen in Table 1, the magnetic coupling in Sr_2CuO_3 is nearly two times larger than that in La_2CuO_4. In both cases, the computation of J is done using only two magnetic centres, so this difference should not be attributed to the dimensionality of the two materials. The other structural difference is the presence of apical oxygen ions in La_2CuO_4, which changes the local multiplet splittings, mainly the position of $3d_{z^2}$ levels[26,40–42]. The relative energy of the $3d_{z^2}$ orbital is believed to be connected to the shape of the Fermi surface and the value of the critical temperature in doped cuprates[43–46].

There is experimental evidence that J also changes depending on the local geometry[47]. However, because different compounds have to be used experimentally, local distortions are accompanied by changes of Cu–O distances and type of adjacent metal ions. Therefore, it is instructive to investigate the dependence of J on the distance to apical oxygen ions in La_2CuO_4 compound with an accurate computational method. We varied the apical O's positions within the cluster while keeping the electrostatic potential untouched and computed magnetic couplings using the procedure described above. The results of these calculations are presented in Fig. 4. It can be seen that, with increase of the distance to apical oxygen, the NN J grows. Moreover, the growth is faster when more electron correlation is taken into account. One obvious effect that leads to an increase of J is the lowering of the $4d_{z^2}$ orbital energy and corresponding enhancement of the orbital breathing. We observe 13% growth of the occupation of $4d_{z^2}$ orbitals upon 0.8 Å displacement of apical oxygens at the CASSCF(24,26) level.

The computational strategy presented and justified here was recently used to predict the superexchange strength in infinite-layer nickelate compounds[48] preceding the consistent experimental studies[49,50].

Online content

Any methods, additional references, Nature Research reporting summaries, source data, extended data, supplementary information, acknowledgements, peer review information; details of author contributions and competing interests; and statements of data and code availability are available at https://doi.org/10.1038/s41567-021-01439-1.

Received: 29 March 2018; Accepted: 27 October 2021;
Published online: 20 December 2021

References

1. Kramers, H. A. L'interaction entre les atomes magnétogènes dans un cristal paramagnétique. *Physica* **1**, 182 (1934).
2. Anderson, P. W. Antiferromagnetism. Theory of superexchange interaction. *Phys. Rev.* **79**, 350 (1950).
3. Zhang, F. C. & Rice, T. M. Effective Hamiltonian for the superconducting Cu oxides. *Phys. Rev. B* **37**, 3759 (1988).
4. Khomskii, D. I. *Transition Metal Compounds* (Cambridge Univ. Press, 2014).
5. van Oosten, A., Broer, R. & Nieuwpoort, W. Heisenberg exchange enhancement by orbital relaxation in cuprate compounds. *Chem. Phys. Lett.* **257**, 207 (1996).
6. Muñoz, D., Illas, F. & de P. R. Moreira, I. Accurate prediction of large antiferromagnetic interactions in high-T_c $HgBa_2Ca_{n-1}Cu_nO_{2n+2\delta}$ ($n=2,3$) superconductor parent compounds. *Phys. Rev. Lett.* **84**, 1579 (2000).
7. de Graaf, C., Sousa, C., d. P. R. Moreira, I. & Illas, F. Multiconfigurational perturbation theory: an efficient tool to predict magnetic coupling parameters in biradicals, molecular complexes, and ionic insulators. *J. Phys. Chem. A* **105**, 11371 (2001).
8. Calzado, C. J., Angeli, C., Taratiel, D., Caballol, R. & Malrieu, J.-P. Analysis of the magnetic coupling in binuclear systems. III. The role of the ligand to metal charge transfer excitations revisited. *J. Chem. Phys.* **131**, 044327 (2009).
9. Fink, K. & Staemmler, V. A modified CAS-CI approach for an efficient calculation of magnetic exchange coupling constants. *Mol. Phys.* **111**, 2594 (2013).

10. Calzado, C. J. & Malrieu, J.-P. Proposal of an extended *t–J* Hamiltonian for high-T_c cuprates from ab initio calculations on embedded clusters. *Phys. Rev. B* **63**, 214520 (2001).
11. Helgaker, T., Jørgensen, P. & Olsen, J. *Molecular Electronic Structure Theory* (Wiley, 2000).
12. Roos, B. O., Taylor, P. R. & Siegbahn, P. E. A complete active space SCF method (CASSCF) using a density matrix formulated super-CI approach. *Chem. Phys.* **48**, 157 (1980).
13. Li Manni, G., Smart, S. D. & Alavi, A. Combining the complete active space self-consistent field method and the full configuration interaction quantum monte carlo within a super-CI framework, with application to challenging metal-porphyrins. *J. Chem. Theory Comput.* **12**, 1245 (2016).
14. Sun, Q., Yang, J. & K.-L. Chan, G. A general second order complete active space self-consistent-field solver for large-scale systems. *Chem. Phys. Lett.* **683**, 291 (2017).
15. Booth, G. H., Thom, A. J. W. & Alavi, A. Fermion Monte Carlo without fixed nodes: a game of life, death, and annihilation in Slater determinant space. *J. Chem. Phys.* **131**, 054106 (2009).
16. Cleland, D. M., Booth, G. H. & Alavi, A. A study of electron affinities using the initiator approach to full configuration interaction quantum Monte Carlo. *J. Chem. Phys.* **134**, 024112 (2011).
17. Sharma, S. & K.-L. Chan, G. Spin-adapted density matrix renormalization group algorithms for quantum chemistry. *J. Chem. Phys.* **136**, 124121 (2012).
18. Angeli, C., Cimiraglia, R. & Malrieu, J.-P. *N*-electron valence state perturbation theory: a fast implementation of the strongly contracted variant. *Chem. Phys. Lett.* **350**, 297 (2001).
19. Sharma, S., Knizia, G., Guo, S. & Alavi, A. Combining internally contracted states and matrix product states to perform multireference perturbation theory. *J. Chem. Theory Comput.* **13**, 488 (2017).
20. Sharma, S. & Alavi, A. Multireference linearized coupled cluster theory for strongly correlated systems using matrix product states. *J. Chem. Phys.* **143**, 102815 (2015).
21. Calzado, C. J., Sanz, J. F. & Malrieu, J. P. Accurate ab initio determination of magnetic interactions and hopping integrals in $La_{2-x}Sr_xCuO_4$ systems. *J. Chem. Phys.* **112**, 5158 (2000).
22. Hozoi, L., Laad, M. S. & Fulde, P. Fermiology of cuprates from first principles: from small pockets to the Luttinger Fermi surface. *Phys. Rev. B* **78**, 165107 (2008a).
23. Gunnarsson, O., Andersen, O. K., Jepsen, O. & Zaanen, J. Density-functional calculation of the parameters in the Anderson model: application to Mn in CdTe. *Phys. Rev. B* **39**, 1708 (1989).
24. Gunnarsson, O. & Jepsen, O. Configuration dependence of hopping matrix elements in the Anderson model. *Phys. Rev. B* **38**, 3568(R) (1988).
25. de Graaf, C. & Broer, R. *Magnetic Interactions in Molecules and Solids* (Springer, 2016).
26. Schlappa, J. et al. Spin-orbital separation in the quasi-one-dimensional Mott insulator Sr_2CuO_3. *Nature* **485**, 82 (2012).
27. Walters, A. C. Effect of covalent bonding on magnetism and the missing neutron intensity in copper oxide compounds. *Nat. Phys.* **5**, 867 (2009).
28. Braicovich, L. et al. Dispersion of magnetic excitations in the cuprate La_2CuO_4 and $CaCuO_2$ compounds measured using resonant X-ray scattering. *Phys. Rev. Lett.* **102**, 167401 (2009).
29. Coldea, R. et al. Spin waves and electronic interactions in La_2CuO_4. *Phys. Rev. Lett.* **86**, 5377 (2001).
30. Malrieu, J. P., Caballol, R., Calzado, C. J., de Graaf, C. & Guihéry, N. Magnetic interactions in molecules and highly correlated materials: physical content, analytical derivation, and rigorous extraction of magnetic hamiltonians. *Chem. Rev.* **114**, 429 (2013).
31. Andersson, K. & Roos, B. O. Excitation energies in the nickel atom studied with the complete active space SCF method and second-order perturbation theory. *Chem. Phys. Lett.* **191**, 507 (1992).
32. Pierloot, K. Transition metals compounds: outstanding challenges for multiconfigurational methods. *Int. J. Quantum Chem.* **111**, 3291 (2011).
33. Li Manni, G. & Alavi, A. Understanding the mechanism stabilizing intermediate spin states in Fe(II)-porphyrin. *J. Phys. Chem. A* **122**, 4935 (2018).
34. Ma, D., Li Manni, G. & Gagliardi, L. The generalized active space concept in multiconfigurational self-consistent field methods. *J. Chem. Phys.* **135**, 044128 (2011).
35. Bar-Deroma, R., Felsteiner, J., Brener, R., Ashkenazi, J. & van der Marel, D. Auger spectra and band structure of $La_{1.85}Sr_{0.15}CuO_4$ and $La_{1.85}Ba_{0.15}CuO_4$. *Phys. Rev. B* **45**, 2361 (1992).
36. Hybertsen, M. S., Schlüter, M. & Christensen, N. E. Calculation of Coulomb-interaction parameters for La_2CuO_4 using a constrained-density-functional approach. *Phys. Rev. B* **39**, 9028 (1989).
37. McMahan, A. K., Martin, R. M. & Satpathy, S. Calculated effective Hamiltonian for La_2CuO_4 and solution in the impurity Anderson approximation. *Phys. Rev. B* **38**, 6650 (1988).
38. Zaanen, J. et al. What can be learned about high T_c from local density theory? *Phys. C.* **153-155**, 1636 (1988).
39. Gunnarsson, O., Jepsen, O. & Shen, Z.-X. Local singlet for CuO and Nd_2CuO_4. *Phys. Rev. B* **42**, 8707 (1990).
40. Moretti Sala, M. et al. Energy and symmetry of *dd* excitations in undoped layered cuprates measured by Cu L_3 resonant inelastic x-ray scattering. *N. J. Phys.* **13**, 043026 (2011).
41. Hozoi, L., Siurakshina, L., Fulde, P. & van den Brink, J. Ab initio determination of Cu 3*d* orbital energies in layered copper oxides. *Sci. Rep.* **1**, 65 (2011).
42. Huang, H.-Y. et al. Ab initio calculation of *d–d* excitations in quasi-one-dimensional Cu d^9 correlated materials. *Phys. Rev. B* **84**, 235125 (2011).
43. Eskes, H. & Sawatzky, G. A. Single-, triple-, or multiple-band Hubbard models. *Phys. Rev. B* **44**, 9656 (1991).
44. Ohta, Y., Tohyama, T. & Maekawa, S. Apex oxygen and critical temperature in copper oxide superconductors: universal correlation with the stability of local singlets. *Phys. Rev. B* **43**, 2968 (1991).
45. Raimondi, R., Jefferson, J. H. & Feiner, L. F. Effective single-band models for the high-T_c cuprates. II. Role of apical oxygen. *Phys. Rev. B* **53**, 8774 (1996).
46. Hozoi, L., Laad, M. S. & Fulde, P. Fermiology of cuprates from first principles: from small pockets to the Luttinger Fermi surface. *Phys. Rev. B* **78**, 165107 (2008b).
47. Peng, Y. Y. et al. Influence of apical oxygen on the extent of in-plane exchange interaction in cuprate superconductors. *Nat. Phys.* **13**, 1201 (2017).
48. Katukuri, V. M., Bogdanov, N. A., Weser, O., van den Brink, J. & Alavi, A. Electronic correlations and magnetic interactions in infinite-layer $NdNiO_2$. *Phys. Rev. B* **102**, 241112 (2020).
49. Lu, H. et al. Magnetic excitations in infinite-layer nickelates. *Science* **373**, 213 (2021).
50. Lin, J. Q. et al. Strong superexchange in a $d^{9-\delta}$ nickelate revealed by resonant inelastic X-ray scattering. *Phys. Rev. Lett.* **126**, 087001 (2021).

Methods

We use clusters that include two CuO_4 (CuO_6) units, two (ten) neighbouring Cu^{2+} ions and all adjacent Sr^{2+} (La^{3+}) ions, in total $[Cu_4O_7Sr_{16}]$ and $[Cu_{12}O_{11}La_{16}]$ for Sr_2CuO_3 and La_2CuO_4, respectively (Supplementary Fig. 1). The rest of the solid is modelled by an array of point charges fitted to reproduce the Madelung potential in the cluster region[51–53]. Further details of the embedded cluster approach including possible improvements[54–60] are presented in Supplementary Note 2. We employed crystal structures as reported experimentally[61,62]. The value of the NN superexchange parameter can be easily extracted by mapping the energy spectrum of the two-magnetic-site cluster to two-site Heisenberg model. To make this mapping straightforward, the peripheral Cu ions are represented by total-ion potentials with no associated electrons, such that J can be extracted as the energy difference of the lowest triplet and singles states[25]. We use all-electron cc-pVDZ and cc-pVTZ basis sets for central Cu and O ions[63,64] and large-core effective potentials for other species[65–67]. We utilize several quantum chemistry computational packages[68–71]. Small CASSCF calculations up to (8,10) active space were done with OpenMolcas, Molpro and PySCF programs[69–71]. Results by different codes are fully consistent with differences in total energies of no more than 10^{-6} Hartree. All NEVPT2 and MR-LCC2 calculations were carried out with IC-MPS-PT and StackBlock programs[17,19]. CASPT2 calculations were performed with OpenMolcas[69]. MRCI-SD and DDCI calculations were done with the 'mrcic'[72] and 'mrci'[73] modules of Molpro[71], respectively. Large CASSCF(24,26) calculations were carried out with OpenMolcas[69] using NECI[68,74,75] as FCIQMC solver[13] and independently with PySCF[70] using StackBlock as DMRG solver[17]. The largest walker number in FCIQMC calculations was set to 10^7. DMRG calculations were carried out with bond dimension $M=3{,}000$. Bond dimension $M=6{,}000$ was used for the uncontracted part of NEVPT2 and MR-LCC2 calculations. To prevent Cu 3*s*, 3*p* and bridging O 2*s* orbitals from entering the active space in CASSCF(28,30) calculations, we keep all orbitals below O 2*p* frozen during the SCF procedure. Further details are provided in Supplementary Methods.

Data shown in Fig. 3 were obtained in constrained calculations using the generalized active space SCF (GASSCF) method[34] as implemented in OpenMolcas[69]. To perform them, we divide the starting atomic-like orbitals into three groups: all *d* orbitals at the first copper ion (15 in cc-pVDZ basis), all *d* orbitals at the second copper ion (15) and the rest. Any orbital rotation between these groups is forbidden via 'super-symmetry' constraint. With GASSCF, we specify two disconnected active spaces, for example, (8,5) and (10,5) for the first and second Cu ion, respectively. This way, it is possible to fix the occupation of *d* orbitals at each site and perform all possible remaining optimizations. The results of GASSCF calculations were cross-checked using ANO-L-VDZP basis set[76,77]. More detail is provided in Supplementary Note 1.

The bare on-site Coulomb interaction between two 3*d* electrons of $U\approx 28$ eV was computed as $U = 2E_{d^9} - E_{d^8} - E_{d^{10}}$ for isolated Cu ion at CASCI level with nine, eight and ten electrons in five orbitals optimized for the d^9 state. The corresponding Coulomb integral $< 3d3d \parallel 3d3d >$ was 29.8 eV in these calculations.

Data for the density plots were obtained using the Multiwfn program[78]. Molecular orbitals and geometries were plotted using Jmol[79] and renmol[80].

Data availability

Data that support the findings of this study are available as a supplementary dataset[81]. Further data are available from the corresponding authors upon reasonable request.

Code availability

NECI code is available at GitHub: https://github.com/ghb24/NECI_STABLE. OpenMolcas code is available at GitLab: https://gitlab.com/Molcas/OpenMolcas. PySCF code is available at GitHub: https://github.com/sunqm/pyscf. StackBlock code is available at GitHub: https://github.com/sanshar/StackBlock. Molpro package can be ordered on its official web site: http://www.molpro.net/. Source code of IC-MPS-PT can be obtained upon reasonable request from S.S.

References

51. Ewald, P. P. Die Berechnung optischer und elektrostatischer Gitterpotentiale. *Ann. Phys.* **369**, 253 (1921).
52. Klintenberg, M., Derenzo, S. & Weber, M. Accurate crystal fields for embedded cluster calculations. *Comput. Phys. Commun.* **131**, 120 (2000).
53. Roos, B. & Wahlgren, U. MADPOT and MADFIT programs (Institute of Theoretical Physics, University of Stockholm, 1969).
54. Birkenheuer, U., Fulde, P. & Stoll, H. A simplified method for the computation of correlation effects on the band structure of semiconductors. *Theor. Chem. Acc.* **116**, 398 (2006).
55. Huang, C., Pavone, M. & Carter, E. A. Quantum mechanical embedding theory based on a unique embedding potential. *J. Chem. Phys.* **134**, 154110 (2011).
56. Bogdanov, N. A., van den Brink, J. & Hozoi, L. Ab initio computation of *d*–*d* excitation energies in low-dimensional Ti and V oxychlorides. *Phys. Rev. B* **84**, 235146 (2011).
57. Barandiarán, Z. & Seijo, L. The ab initio model potential representation of the crystalline environment. Theoretical study of the local distortion on NaCl:Cu^+. *J. Chem. Phys.* **89**, 5739 (1988).
58. Winter, N. W., Pitzer, R. M. & Temple, D. K. Theoretical study of a Cu^+ ion impurity in a NaF host. *J. Chem. Phys.* **86**, 3549 (1987).
59. Bogdanov, N. A., Katukuri, V. M., Stoll, H., van den Brink, J. & Hozoi, L. Post-perovskite $CaIrO_3$: a $j=1/2$ quasi-one-dimensional antiferromagnet. *Phys. Rev. B* **85**, 235147 (2012).
60. Lepetit, M.-B., Suaud, N., Gelle, A. & Robert, V. Environment effects on effective magnetic exchange integrals and local spectroscopy of extended strongly correlated systems. *J. Chem. Phys.* **118**, 3966 (2003).
61. Hyatt, N. C., Gray, L., Gameson, I., Edwards, P. P. & Hull, S. High-pressure neutron diffraction study of the quasi-one-dimensional cuprate Sr_2CuO_3. *Phys. Rev. B* **70**, 214101 (2004).
62. Cava, R. J., Santoro, A., Johnson, D. W. & Rhodes, W. W. Crystal structure of the high-temperature superconductor $La_{1.85}Sr_{0.15}CuO_4$ above and below T_c. *Phys. Rev. B* **35**, 6716 (1987).
63. Dunning Jr., T. H. Gaussian basis sets for use in correlated molecular calculations. I. The atoms boron through neon and hydrogen. *J. Chem. Phys.* **90**, 1007 (1989).
64. Balabanov, N. B. & Peterson, K. A. Systematically convergent basis sets for transition metals. I. All-electron correlation consistent basis sets for the 3*d* elements Sc–Zn. *J. Chem. Phys.* **123**, 064107 (2005).
65. Fuentealba, P., von Szentpály, L., Preuss, H. & Stoll, H. Pseudopotential calculations for alkaline-earth atoms. *J. Phys. B* **18**, 1287 (1985).
66. Dolg, M., Stoll, H., Savin, A. & Preuss, H. Energy-adjusted pseudopotentials for the rare earth elements. *Theor. Chim. Acta* **75**, 173 (1989).
67. Dolg, M., Stoll, H. & Preuss, H. A combination of quasirelativistic pseudopotential and ligand field calculations for lanthanoid compounds. *Theor. Chim. Acta* **85**, 441 (1993).
68. Booth, G. H., Smart, S. D. & Alavi, A. Linear-scaling and parallelisable algorithms for stochastic quantum chemistry. *Mol. Phys.* **112**, 1855 (2014).
69. Fdez Galván, I. et al. OpenMolcas: from source code to insight. *J. Chem. Theory Comput.* **15**, 5925 (2019).
70. Sun, Q. et al. PySCF: the Python-based simulations of chemistry framework. *WIREs Comput. Mol. Sci.* **8**, e1340 (2017).
71. Werner, H.-J., Knowles, P. J., Knizia, G., Manby, F. R. & Schütz, M. Molpro: a general-purpose quantum chemistry program package. *WIREs Comput. Mol. Sci.* **2**, 242 (2011).
72. Shamasundar, K. R., Knizia, G. & Werner, H.-J. A new internally contracted multi-reference configuration interaction method. *J. Chem. Phys.* **135**, 054101 (2011).
73. Werner, H. & Knowles, P. J. An efficient internally contracted multiconfiguration-reference configuration interaction method. *J. Chem. Phys.* **89**, 5803 (1988).
74. Ghanem, K., Guther, K. & Alavi, A. The adaptive shift method in full configuration interaction quantum Monte Carlo: development and applications. *J. Chem. Phys.* **153**, 224115 (2020).
75. Guther, K. et al. NECI: *N*-electron configuration interaction with an emphasis on state-of-the-art stochastic methods. *J. Chem. Phys.* **153**, 034107 (2020).
76. Widmark, P.-O., Malmqvist, P.-Å & Roos, B. O. Density matrix averaged atomic natural orbital (ANO) basis sets for correlated molecular wave functions. *Theor. Chim. Acta* **77**, 291 (1990).
77. Pou-Amérigo, R., Merchán, M., Nebot-Gil, I., Widmark, P.-O. & Roos, B. O. Density matrix averaged atomic natural orbital (ANO) basis sets for correlated molecular wave functions. *Theor. Chim. Acta* **92**, 149 (1995).
78. Lu, T. & Chen, F. Multiwfn: a multifunctional wavefunction analyzer. *J. Comput. Chem.* **33**, 580 (2012).
79. Jmol: an open-source Java viewer for chemical structures in 3D; http://www.jmol.org/
80. Knizia, G. renmol: molecules and pictures. *Penn State University* https://sites.psu.edu/knizia/software/ (2017).
81. Bogdanov, N. A., Li Manni, G., Sharma, S., Gunnarsson, O. & Alavi. A. Supplementary dataset for: Enhancement of superexchange due to synergetic breathing and hopping in corner-sharing cuprates. *Zenodo* https://doi.org/10.5281/zenodo.5590408 (2021).

Acknowledgements

The authors gratefully acknowledge financial support from the Max Planck Society. N.A.B. thanks D. Kats for helping with the Molpro package and L. Hozoi for fruitful discussions. S.S. was supported by NSF grant CHE-1800584 and Sloan Research Fellowship. Part of the computations were carried out at the Max Planck Computing and Data Facility (MPCDF).

Author contributions

N.A.B. and A.A. designed the project. N.A.B. and G.L.M. designed the active space strategy for this work. N.A.B. carried out the ab initio calculations with contributions from G.L.M. and S.S. G.L.M. developed and adapted the stochastic CASSCF and GAS approaches to the present study. S.S. developed and adjusted for the present study computer programs to perform MR-LCC2 and NEVPT2 computations with large active

spaces. O.G. carried out the model Hamiltonian analysis. N.A.B., O.G. and A.A. wrote the paper with contributions from all other co-authors;

Funding
Open access funding provided by Max Planck Society.

Competing interests
The authors declare no competing interests.

Additional information
Supplementary information The online version contains supplementary material available at https://doi.org/10.1038/s41567-021-01439-1.

Correspondence and requests for materials should be addressed to Nikolay A. Bogdanov or Ali Alavi.

Peer review information *Nature Physics* thanks the anonymous reviewers for their contribution to the peer review of this work